Supplemental Materials

Figure S1. Characterization of FcRL5$^+$T-bet$^+$ Bmem cell subsets, Related to Figure 1.

(**A-B**) B lineage subsets in peripheral blood of HD (n=19) immunized with IIV. Representative flow cytometry plots (**A**) defining the CD38^{hi}CD27^{hi} PB population, IgD$^+$CD27^{neg}, IgD^{neg} B cells and naïve B cells are shown. Enumerated PBs on D0 and D7 post-IIV (**B**) shown as frequency of PBs within the total live CD19$^+$ B cell subset for each HD. **p<0.001 paired Student's t-test.

(C-E) Histogram (**C**) from Lau *et al*.[14] showing T-bet expression in circulating CD21^{lo} HA-specific (solid blue line) Bmem cells populations on D14 post-IIV. Expression of CD21 versus T-bet (**D**) by D7 HA-specific IgD^{neg} B cells. CD21^{hi} cells are denoted in a green box and CD21^{lo} cells are denoted in a blue box. Expression of CD71 versus T-bet (**E**) by HA-specific IgD^{neg} B cells. CD71$^+$ cells are denoted in a green box and CD71^{neg} cells are denoted in a purple box.

(**F-J**) Distribution of V_H sequence mutation frequencies in sort-purified H3-specific IgD^{neg} FcRL5$^+$ and FcRL5^{neg} B cells. Frequencies reported as mutations relative to IMGT germline per 100 nucleotides (nt) in the CDR1+CDR2 regions (**F**), or the FR1+FR2+FR3 regions (**G**) considering all isotypes, or the V_H region (**H**), the CDR1+CDR2 regions (**I**) or the FR1+FR2+FR3 regions (**J**), considering only IgA and IgG sequences. Number of sequences in each population indicated.

(**K-M**) HA-specific IgD^{neg} B cells were enumerated from blood of HD (n= 8) at D120 post-IIV. FACS plots from representative HD showing HA-specific IgD^{neg} B cells (**K**) and expression of T-bet and FcRL5 (**L**) by the HA- specific IgD^{neg} subset. Frequencies of T-bet$^+$ and T-bet^{neg} B cells (**M**) within the H1-specific or H3-specific IgD^{neg} B cell compartment. Statistical analysis performed using Wilcoxon matched-pairs signed rank test.

(**N**) Shared lineages between D7 H3-specific IgD^{neg} FcRL5$^+$ and FcRL5^{neg} Bmem cells isolated from 2 HDs. Data represented as alluvial plots with the individual lineages ranked by size in each subset. Total number of non-singleton lineages indicated at the bottom of each bar. Non-singleton lineages shared between the Bmem cell subsets shown as ribbons. See Table S1 for all BCR repertoire data.

Figure S2. Molecular Characterization of FcRL5$^+$T-bet$^+$ Bmem cell subsets, related to Figure 2.

RNA-seq and ATAC-seq analyses performed on sort-purified circulating PB (green), naïve B cells (brown), H1-specific IgD^{neg} FcRL5^{neg} (blue) cells and H1-specific IgD^{neg} FcRL5$^+$ B cells (red) from HD on D7 (**A-B**, n=6 HD) or D14 (**C-I**, n=4 HD) post-IIV.

(**A-B**) RNA expression in RPKM (**A**) for *TBX21* and *FCRL5* in D7 H1-specific IgD^{neg} FcRL5$^+$ and FcRL5^{neg} B cells. RNA expression (**B**) of cell cycle genes (Table S2) in D7 B cell subsets represented as a heat map of per-gene z-score of log gene expression.

(**C-D**) GSEA (**C**) comparing the RNA-seq ranked gene list from D14 CD19$^+$CD27$^+$CD38$^{lo/med}$ CD21^{lo} vs CD21^{hi} B cells[14] to known plasma cell-specific IRF4 targets[18]. Venn diagrams (**D**) showing overlap

between the 262 DEG identified in D14 CD19^{+} CD38$^{lo/med}$ CD27^{+}CD21^{lo} vs CD21^{hi} B cells[14] (Table S2) and the 394 DEGs identified in D14 H1-specific IgD^{neg} FcRL5^{+} vs FcRL5^{neg} Bmem cells (Table S2).

(**E-F**) PCA for the D14 RNA-seq (4,889 DEG) (**E**) and ATAC-seq (19,775 DAR) (**F**) data sets from each B cell subset using the indicated DEG or DAR that were different across the data sets.

(**G**) Chromatin accessibility surrounding IRF4 ASC regulon genes[18] (Table S2) as assessed in D14 ATAC-seq datasets. Data, reported as RPPM, represent mean peak accessibility for all peaks mapping to genes directly regulated by IRF4 in plasma cells.

(**H-I**) PR identified transcriptional regulators of D7 PBs, D14 H1-specific IgD^{neg} FcRL5^{+} and D14 H1-specific IgD^{neg} FcRL5^{neg} gene networks (Table S2). Comparison between the D14 FcRL5^{+} Bmem cells over PB (**H**) or D14 FcRL5^{neg} Bmem cells over PBs (**I**) with individual TFs indicated. Statistical analyses were performed using Wilcoxson matched pairs signed rank test (**A)** or two tailed t-testing (**G**). *p< 0.05, **, p<0.01, *** p<0.001, **** p <0.0001 ns= non-significant. p_{nom} values for GSEA analyses indicated.

Figure S3. Transcriptional metabolic pathways activated in FcRL5^{+}T-bet^{+} Bmem cell subsets, related to Figure 5.

(A) GSEA comparing the RNA-seq ranked gene list from D7 H1-specific IgD^{neg} FcRL5^{+} and FcRL5^{neg} B cells to 3931 GO gene lists. Leading edge genes from 185 GO gene lists that were enriched (FDR q-value < 0.01) for expression in FcRL5^{+} relative to the FcRL5^{neg} Bmem cells were used for multidimensional scaling and clustered to group terms that similarly drove enrichment (9 clusters (referred to as A-I, Table S2; see methods). Eleven prototypic GO gene lists (referred to as *i-xi*) representing the 9 GO gene set clusters were selected (Table S2). Relationships between the 11 Prototype GO lists (*i-xi*, rows) and the 9 clusters (A-I, columns) are indicated. Some GO lists were associated with more than 1 cluster (blue, primary cluster and grey, secondary cluster) and more than 1 prototypic GO list was identified for some clusters.

(**B-O**) The leading-edge genes from the 11 prototypic GO gene lists were curated and assigned to 14 signaling and metabolic modules (Table S2). Log_2 difference in expression of genes assigned to the 14 modules in the D7 H1-specific IgD^{neg} FcRL5^{+}and FcRL5^{neg} Bmem cell samples from individual donors. FDR q<0.05 (red dots) or FDR q>0.05 (black dots) in the FcRL5^{+} over FcRL5^{neg} comparison. Vertical black bars indicate functional subdivisions within each module.

Figure S4. Functional characterization of FcRL5^{+}T-bet^{+} Bmem cell subsets, related to Figure 6.

(**A-C**) Identification of FcRL5^{+} (T-bet expressing) and FcRL5^{neg} (T-bet^{neg}) IgD^{neg}CD27^{+} Bmem cells in tonsil. Non-GC, Ag-experienced CD38^{lo}IgD^{neg} CD19^{+} tonsil B cells were gated (**A**) and analyzed for expression of CD27, FcRL5 and T-bet (**B-C**).

(**D-G**) Metabolic analyses of tonsil-derived matched FcRL5^{+} (red) and FcRL5^{neg} (blue) IgD^{neg}CD27^{+} Bmem cells showing representative histograms of FcRL5^{+} and FcRL5^{neg} cells from the same donor. ROS

activity (**D**) assessed following staining with 2, 7 – dichlorohydrofluorescein diacetate (H_2DCF). Mitochondrial mass **(E)** as measured by staining with Mitotracker Green. Membrane lipid analysis **(F)** as measured by staining with the fatty acid analog BODIPY510. mTORC1 activation **(G)** as measured by expression of phosphorylated S6 (pS6) kinase. Gray histograms indicate naïve B cells (**D-F**) or isotype control staining (**G**).

(**H-N**) *In vitro* proliferation and differentiation assays with tonsil Bmem cell subsets. Donor-matched sort-purified naïve (brown), and IgD^{neg}CD27^{+}CD38$^{lo/med}$ Bmem cell subsets (CD27^{+}FcRL5^{+} (red), CD27^{+}FcRL5^{neg} (blue), CD27^{neg}FcRL5^{+} (magenta), CD27^{neg}FcRL5^{neg} (aqua)) (see Fig. S4A-C for sorting strategy), labeled with CTV, stimulated with R848, IL-21, IL-2 and IFN-γ and assessed on D2 (**M-N,** n=2 donors) or D3 (**H-L**, n = 3 donors). Cell survival (**H**), frequencies of cells in each cell division (**I**), frequencies of total CD27^{hi}CD38^{hi} ASCs (J-K, M-N) and percentage of ASCs in each cell division (**L**) shown.

Statistical analyses were performed using one-way ANOVA with Tukey's multiple comparison testing (**H, K**). *p< 0.05, **, p<0.01, *** p<0.001, **** p <0.0001 ns= non-significant

Figure S5. Intracellular Ig expression by FcRL5^{+}T-bet^{+} Bmem cell subsets, related to Figure 6.

(**A**) RNA expression by D7 post-IIV B cell subsets of genes reported[35] to be induced by the mTORC1-dependent early UPR in mouse follicular B cells (Table S2). Genes upregulated in the B cell activation UPR (green circles**)** and the early PC inductive UPR (orange circles) displayed in a heat map showing per-gene z-score of log expression in D7 naïve B cells, FcRL5^{neg} and FcRL5^{+} Bmem cells and PBs.

(**B**) Published FACS plots[2] showing circulating HA-specific B cells over 9 weeks post-seasonal IIV. HA-binding B cells analyzed in the publication[2] are indicated in the blue asterisk denoted grey box (HA^{++} B cells). HA^{int}-binding B cells indicated in red box that we superimposed on the original figure.

(**C**) BCRs expressed by FcRL5^{+} and FcRL5^{neg} HA-specific Bmem cells exhibit similar HA-binding profiles. Single CA09-H1^{+} IgD^{neg} B cells from D7 post-IIV (2017) HD were index-sorted and identified as either FcRL5^{+} (n=202 cells) or FcRL5^{neg} (n=68 cells). Recombinant IgG1 monoclonal Abs (rmAb) from sorted single cells were screened for binding (Table S5) to recombinant H1 Ags arrayed on cytometric beads (CBA assay). Binding reactivities for each rmAb to CA09-H1, MI15-H1, and PR8-H1 Ags are shown as violin plots. ns=non-significant.

(**D**) Binding of rmAbs in CBA assay correlates with the affinity of binding by rmAbs. HA-specific rmAbs (n=8) were generated as described above and analyzed for binding to recombinant HA-CA09 using CBA assay and Surface Plasmon Resonance (SPR) assay. Data shown as the SPR-derived affinity (reported as K_D) of rmAb binding to HA-CA09 plotted against the normalized MFI of rmAb binding to HA-CA09 conjugated beads. The Pearson correlation coefficient is provided.

(**E**) RNA-seq analysis of IgG locus transcripts from sort-purified D7 IgD^{neg} HA-specific FcRL5^{neg} and FcRL5^{+} Bmem cells (N=6 subjects). The median ratio (95% CI) of transmembrane to secretory splice

variants among isotype-switched IgG transcripts (*IgHG1, IgHG2, IgHG3, IgHG4)* is depicted. Statistical analyses performed using Wilcoxon matched-pairs signed rank test.

Figure S6. Durability of FcRL5^{+}T-bet^{+} Bmem cell subsets, related to Figure 7.

Correlation analyses comparing vaccine-elicited D7 PB and Bmem cells from D7 and D14, measured as frequency of indicated populations in blood (x-axis), to vaccine H1- or H3-specific Ab responses, measured as FC (y-axis) in titers between D0 and D120, after IIV in HD (n=19). Comparisons include: FC in H1-specific (circles) or H3-specific (gray squares) IgG titers and the frequency of total D7 PBs present within the CD19^{+} B cell subset (**A**); FC in H1-specific IgG titers and the frequency of the D14 H1-specific T-bet^{neg} Bmem cells (**B**); FC in H3-specific IgG titers and the frequency of the D14 H3-specific T-bet^{neg} Bmem cells (**C**); FC in H1-specific IgG titers and the frequency of the D14 H1-specific T-bet^{+} Bmem cells (**D**); FC in H3-specific IgG titers and the frequency of the D14 H3-specific T-bet^{+} Bmem cells (**E**); FC in *H1-specific* IgG titers and the frequency of the D7 *H3-specific* T-bet^{+} Bmem cells (**F**); and FC in *H3-specific* IgG titers and the frequency of the D7 *H1-specific* T-bet^{+} Bmem cells (**G**). ns = no significant correlation in indicated comparisons. Spearman correlation (r) and significance (p) between indicated correlations are shown.

Supplemental 1

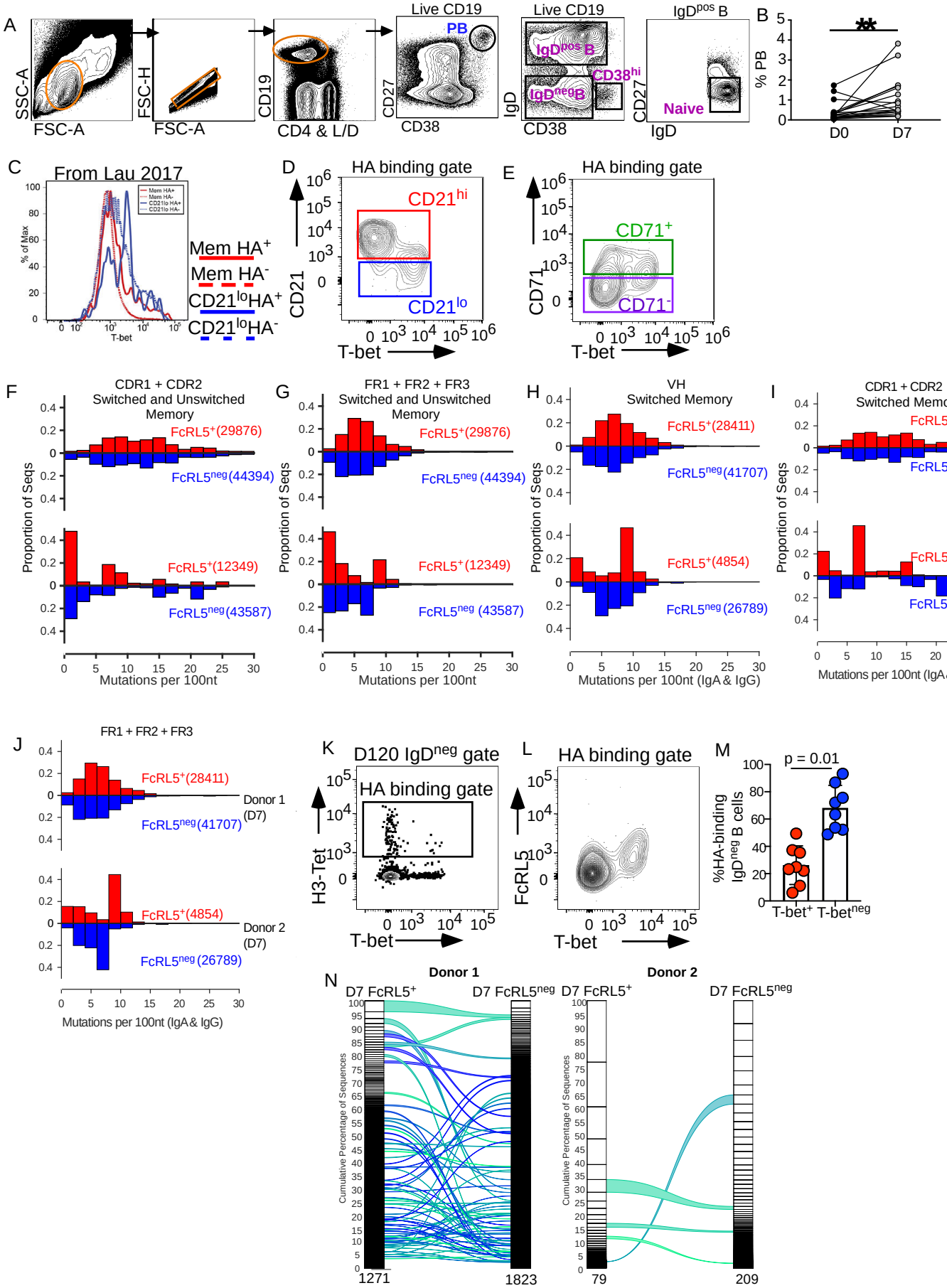

Supplemental 2

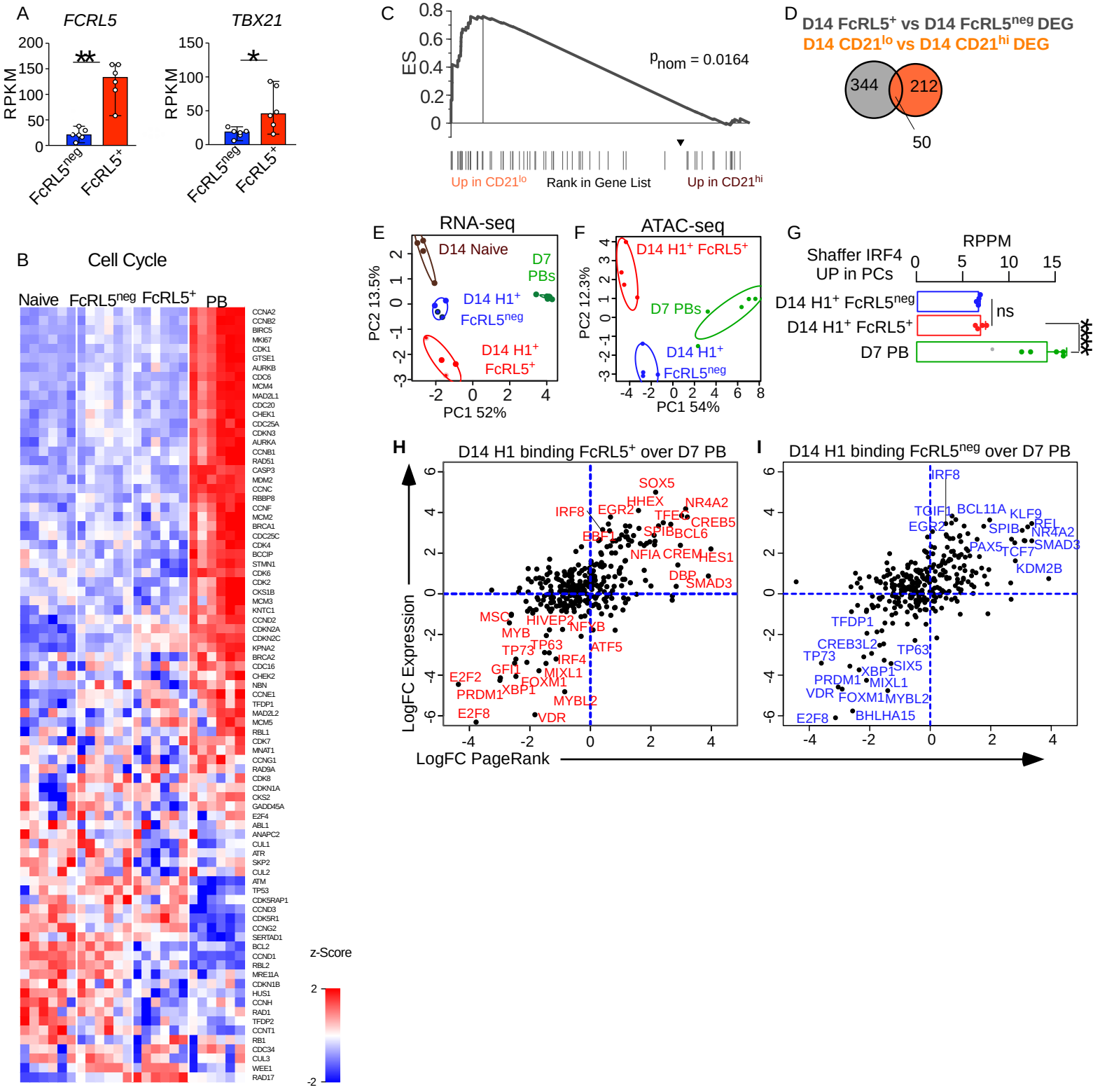

Supplemental 3

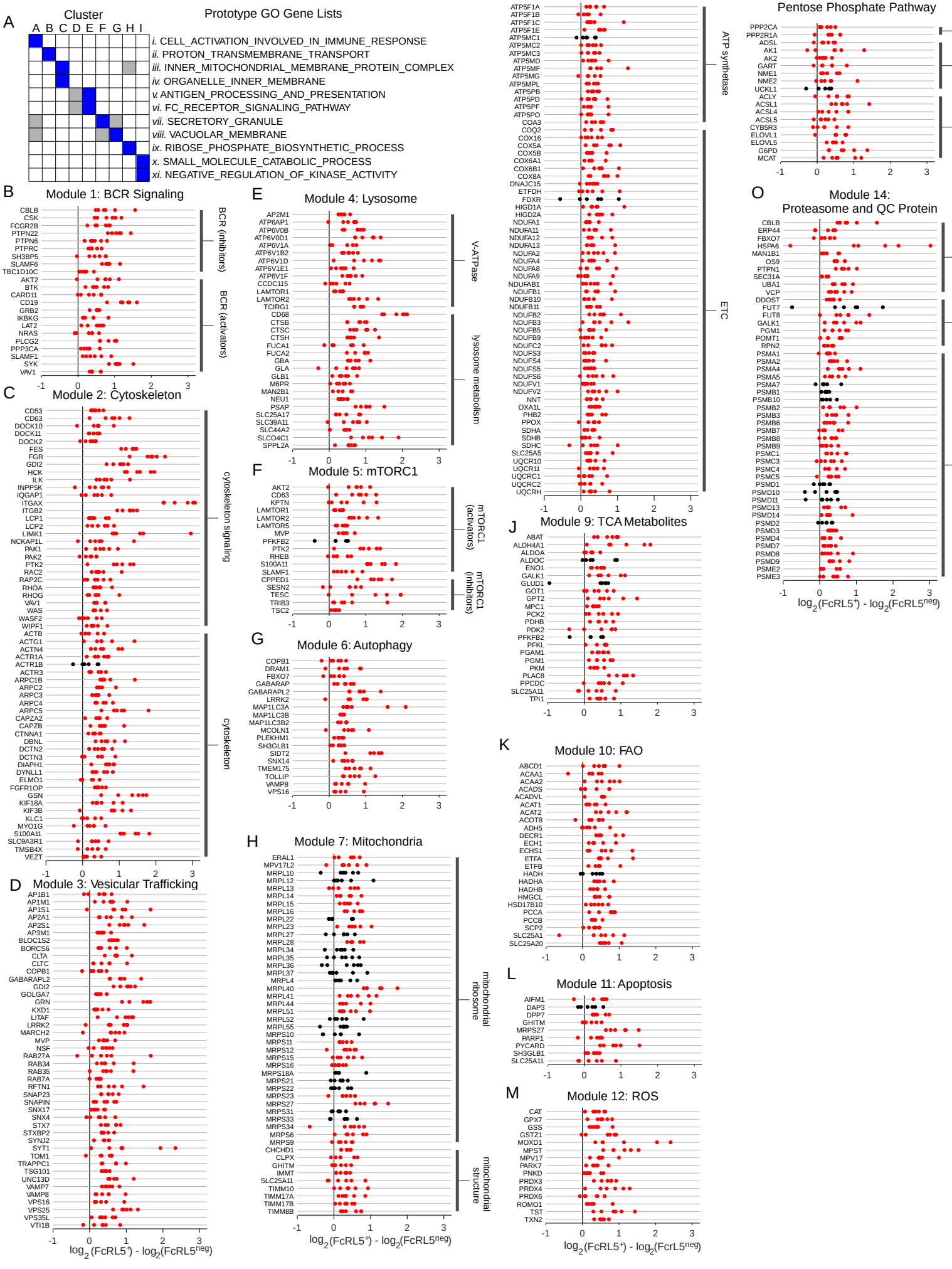

Supplemental 4

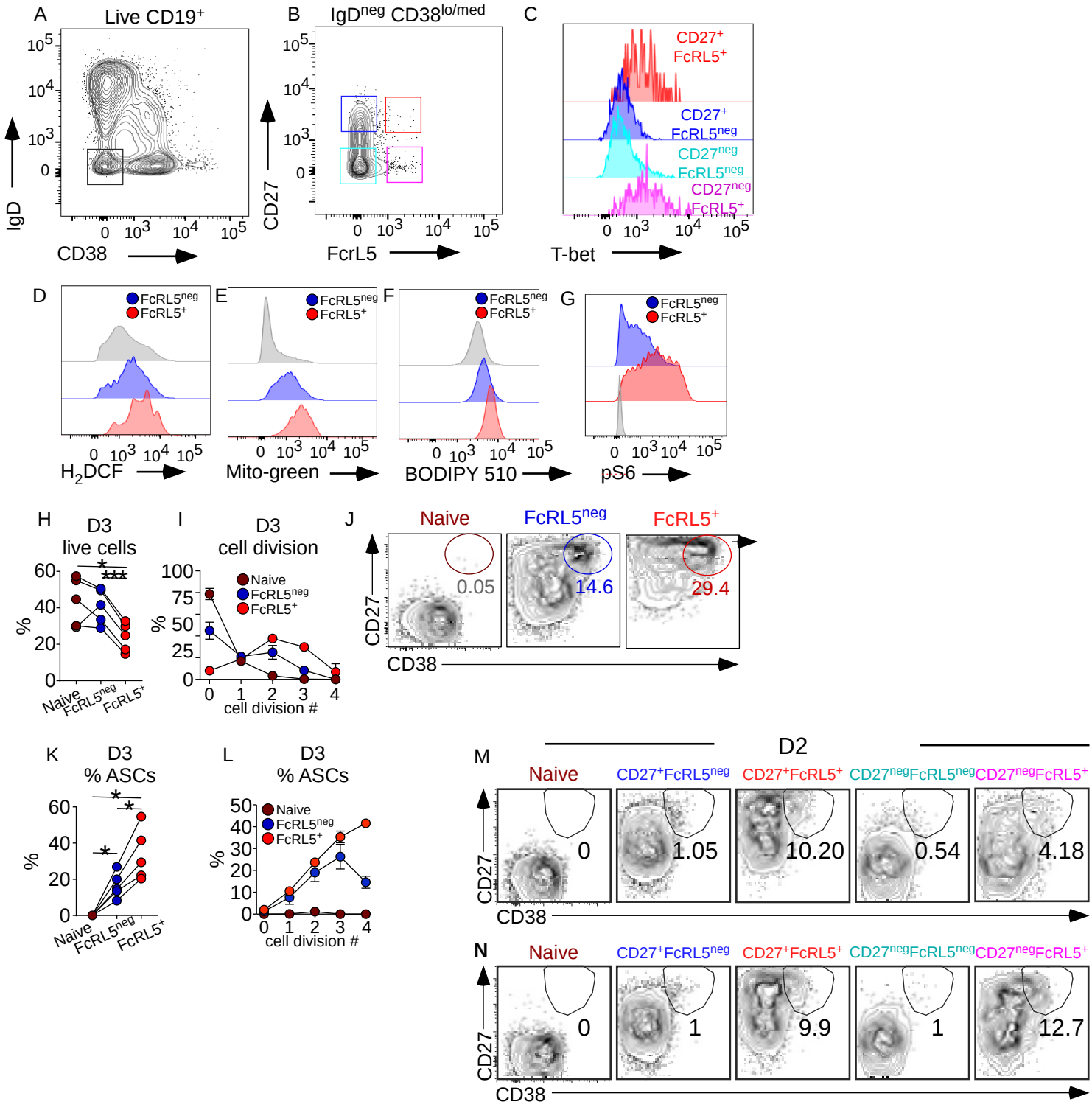

Supplemental 5

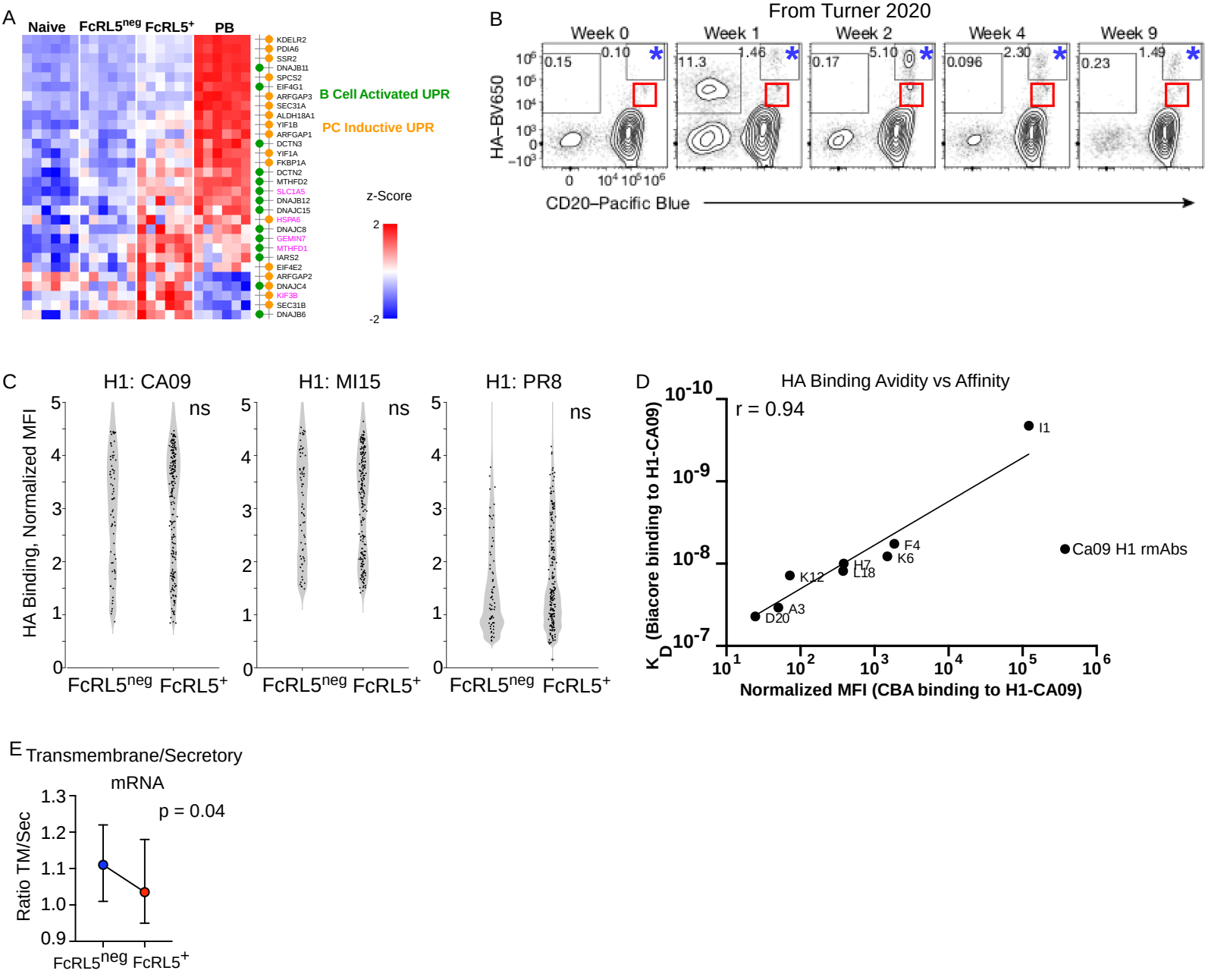

Supplemental 6